

RESEARCH ARTICLE

High photo-conversion efficiency in double-graded Cu(In,Ga)(S,Se)₂ thin film solar cells with two-step sulfurization post-treatment

Gee Yeong Kim¹, JungYup Yang^{2,3}, Trang Thi Thu Nguyen¹, Seokhyun Yoon¹, Junggyu Nam³, Dongho Lee³, Dongseop Kim³, Minsu Kwon⁴, Chan-Wook Jeon⁴, Yoon-Koo Kim⁵, Seung-Yong Lee⁵, Miyoung Kim⁵ and William Jo^{1*}

¹ Department of Physics and New and Renewable Energy Research Center, Ewha Womans University, Seoul, 03760, Korea

² Department of Physics, Kunsan National University, Kunsan, 54150, Korea

³ Photovoltaic Development Team, Samsung SDI, Cheonan, 31086, Korea

⁴ Department of Chemical Engineering, Yeungnam University, Gyeongsan, 38541, Korea

⁵ Department of Materials Science and Engineering, Seoul National University, Seoul, 08826, Korea

ABSTRACT

Sulfur is extensively used to increase the bandgap of Cu(In,Ga)(S,Se)₂ (CIGS_{Se}) solar cells and to improve the open circuit voltage (V_{OC}) in order to optimize the characteristics of the devices. This study uses a sulfurization process to obtain a double-graded bandgap profile. Selenization was carried out on Cu(In,Ga) precursors, followed by one sulfurization process or two consecutive sulfurization processes on top of the CIGS_{Se} absorber layer surface. The optimum two-step sulfurization process provides an increase of V_{OC} of 0.05 V and an improvement of conversion efficiency of 1.17%. The efficiency of the 30 × 30 cm² monolithic module, which has 64 CIGS cells connected in series (aperture area: 878.6 cm²), is 15.85%. The optical and electrical properties of the phase and the work function distribution were investigated using the depth profiles of the absorber layer as a function of the sulfurization conditions. The CIGS_{Se} thin film formed by two-step sulfurization with a high sulfur concentration exhibits a single work function peak, better crystallinity, and higher conversion efficiency than those of the thin film formed by two-step sulfurization at low sulfur concentration. In terms of the Raman spectra depth profile, the phase areas for the CIGS_{Se} thin film that underwent the optimized high sulfur concentration two-step-sulfurization appeared to have less of Cu_{2-x}Se phase than that with low sulfur concentration. Consequently, surface and interface phase analysis is an essential consideration to improve cell efficiency. Copyright © 2016 John Wiley & Sons, Ltd.

KEYWORDS

CIGS_{Se} solar cell; bandgap grading; Kelvin probe force microscopy; Raman scattering spectroscopy

*Correspondence

William Jo, Department of Physics and New and Renewable Energy Research Center, Ewha Womans University, Seoul 03760, Korea
E-mail: wmjo@ewha.ac.kr

Received 21 March 2016; Revised 31 July 2016; Accepted 23 August 2016

1. INTRODUCTION

The highest conversion efficiency that has been achieved for polycrystalline Cu(In,Ga)Se₂ (CIGSe) thin film solar cells is of 22.3% [1], and the highest efficiency of CIGSe modules is 18.7 ± 0.6% for a mini-module size of 15.892 cm² [2]. However, CIGSe solar cells with a larger module size exhibit a lower conversion efficiency, and one of the critical issues for CIGSe thin film solar cells is the bandgap gradient. Most device parameters are determined by the characteristics of the absorber layer, so many research groups have tried to form a Cu(In,Ga)(S,

Se)₂ (CIGS_{Se}) absorber layer with a graded bandgap by controlling the Ga/(Ga + In) and S/(S + Se) ratio [3,4]. The Ga/(Ga + In) ratio of a CIGSe solar cell is important in order to determine device performance, including the open circuit voltage (V_{OC}) and short circuit current density (J_{SC}) [5,6]. Solar Frontier Inc. reported on a solar module made of CIGS_{Se} with 17.8% efficiency, constructed on a 900-cm² module [7,8] where the absorber layer in the module was fabricated via sputtering and an Se and S annealing process. Recently, Samsung SDI achieved an efficiency of 17.9% with a 30 × 30-cm² CIGS_{Se} solar cell [9]. One critical factor that determines the device

performance is the sulfurization process that is used. A surface sulfurization process can produce a high V_{OC} , but strong sulfurization can negatively impact the fill factor of the device. Therefore, it is important to optimize and control the sulfurization process in the CIGSse absorber layer in order to obtain a high-efficiency module.

In this study, we compare a CIGSse film sulfurized in two steps with different H₂S gas concentrations. We characterized the phase distribution of the CIGSse film using the depth profiles, and we discuss the sulfur reaction and phase difference with respect to the sulfurization process. In a previous study, Fontané *et al.* used in-depth resolved Raman spectroscopy and secondary neutral mass spectrometry to investigate the inhomogeneities in a polycrystalline CIGSe layer¹⁰. They prepared a sputter-erosion CIGSe sample with an Ar⁺ beam to obtain the Raman spectra, and compositional inhomogeneity measurements and the Raman spectra were obtained at different depths [10]. Moreover, Fontané *et al.* also obtained micro-Raman spectra with depth profiles from different Cu-poor CuInSe₂ (CIS) thin films, and their results have suggested that secondary phases at the back interface region could influence the electrical characteristics of the back contact in the cells [11]. In this study, the work function distribution was measured from the sample surface to the back contact region to obtain the double bandgap gradient and the phase distribution of the CIGSse thin film as a function of the different sulfurization processes.

2. EXPERIMENTAL

2.1. Growth of CIGSse thin film solar cells

A two-stage process was applied as the growth method for the CIGSse absorber layer. Cu:Ga targets (Cu 28wt.%Ga alloy) and In were sequentially deposited on 300-nm-thick Mo-coated soda lime glass by DC sputtering using a Cu/(Ga+In) ratio of 0.87. Ga metal was deposited near the back contact region to obtain a high bandgap and to thereby form a back electric field. A Cu/(Ga+In) ratio of 0.87 was used, and after growing the film, CIGSse was formed via selenization and sulfurization using H₂Se and H₂S gas, respectively, mixed with N₂ gas. The CIG precursors were first selenized at 500 °C for 35 min with H₂Se (2%) and N₂ gas to form a CIGSe layer, after which the CIGSe films were sulfurized with H₂S and N₂ gas. The surface sulfurization process could be achieved by grading the bandgap near the film surface (front grading). The CIGSse samples were fabricated using two steps with different S concentrations. In the first sulfurization step, we used a ratio of either 0.05 (“low” S concentration; H₂S:N₂=0.05:10) or 2 (“high” S concentration; H₂S:N₂=2:10) H₂S gas for 30 min. The second step used 10% H₂S gas for 30 min. A detailed description of the process creating the CIGSe absorber layer has been previously reported [12,13], and the details of the precursor

deposition and the annealing process are schematically shown in Figure 1. The selenization process included annealing at 500 °C, and for this study, the sulfurization process was controlled as a two-step process. In the two-step sulfurization process, exposure to the H₂S gas was divided into two 30 min periods with first a “low”/“high” S concentration and then a 10% H₂S exposure. A graded bandgap CIGSse absorber was obtained, and its nature was dependent upon the selenization and sulfurization processes that were used. We have studied the sulfurization process over a broad range of temperatures, gas concentrations, and process times. Although the difference between the “low” and “high” contents of H₂S used in the sulfurization process seems minor, the device parameters were very sensitive to sulfurization conditions. In the first sulfurization step, the grain size of the absorber material was improved by using a low concentration of H₂S gas, which diffused into the grain boundaries during the second sulfurization step. If the first sulfurization step is performed under only inert gas (such as N₂ or Ar), many voids form across the CIGSse film. In contrast, too much S in the first step induces defects in the CIGSse surface. Sulfurization with a high H₂S concentration negatively affected both the fill factor and V_{OC} because of the deterioration of P/N junction quality caused by S surface etching. A buffer layer of Zn(O,OH,S) was then grown on the absorber by chemical bath deposition. A transparent conducting oxide layer of boron-doped zinc oxide was subsequently deposited on the Mo/CIGSse/Zn(O,OH,S) film via low-pressure chemical vapor deposition.

2.2. Characterization of CIGSse absorber layer

The CIGSse films were cut on the vicinal plane using a dimpling grinder, whereupon we could observe the phase distribution as a function of the film depth. We used an excitation laser with a wavelength of 488 nm (sapphire-laser) and a spot size of 1 μm. The results of the micro Raman scattering spectra were measured using a spectrometer (Model 207, McPherson Inc.) equipped with a nitrogen-cooled charge-coupled device array detector. We observed phase distribution of CIGSse thin films by micro Raman scattering measurements with an excitation of a 488 nm-wavelength laser operating at a power of 1.5 mW and a spot size of 1 μm in diameter. The cross-sectional views and mapping images of each element were obtained via transmission electron microscopy (JEM-2100 F, JEOL Ltd, Japan) and energy dispersive spectroscopy (EDS). Kelvin probe force microscopy (KPFM) was used to characterize the phase of the sample surface, and further imaging was performed using an atomic force microscope (AFM) (n-Tracer, NanoFocus Inc., Seoul, Korea) with a cantilever with Pt/Ir-coated silicon tips (Nanosensor). The tip was calibrated with highly-oriented pyrolytic graphite ($\Phi=4.6\pm0.1$ eV) to convert the potential difference to a workfunction [14,15] and an absolute workfunction of the

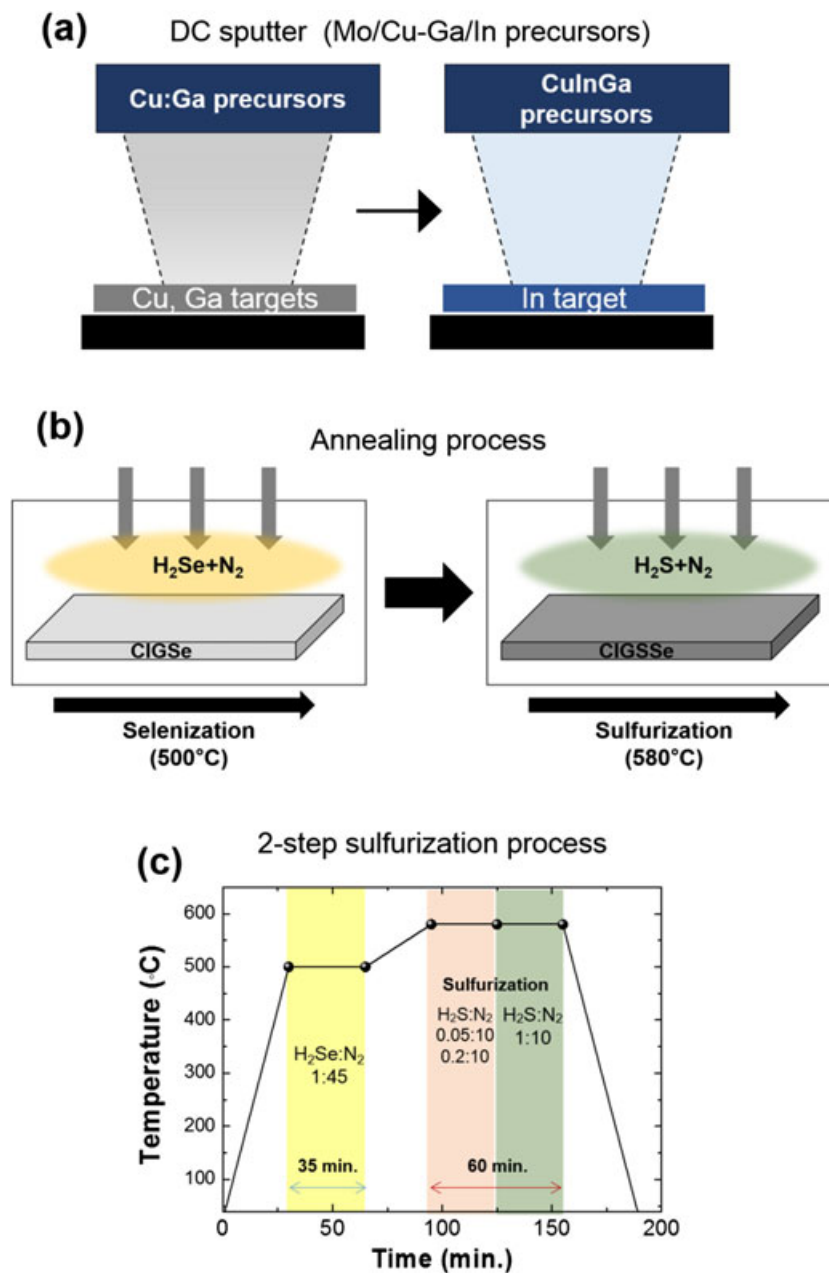


Figure 1. Growth process of the CIGSe absorber layer. (a) The CIG precursors were established with Cu:Ga precursor deposition, followed by In precursor deposition. (b) The precursors were annealed with H₂Se and N₂ gas, after which sulfurization was carried out with H₂S and N₂ gases. (c) The temperature profile of the sulfurization and selenization process for the two-step sulfurization process.

tip. The AFM topographical images were obtained at a probe resonant frequency of 78.18 kHz, and the surface potential was measured in the non-contact mode by applying an AC voltage with amplitude of 1.0 V and a frequency of 60.5 kHz to obtain clear images with sufficient sensitivity. The AFM scan area was of $3 \times 3 \mu\text{m}^2$, and the scanning rate was set to 0.5 Hz to minimize the topological

signal, while the lock-in amplifier operated at a sensitivity of 100 mV/nA. The samples were not damaged while carrying out these AFM measurements. The plane morphology and cross-section of the system were imaged via field emission scanning emission microscopy, while the depth profile composition of the CIGSSe films was characterized using a glow discharge optical emission spectrometer.

3. RESULTS

3.1. CIGSSe growth conditions

Figure 1(a) shows the schematics of the deposition process for the absorber layer. The Solar Frontier group (SF) have previously reported on the sulfurization conditions of a CIGSSe film [7,8] that are similar to those used in this work, though there are some differences. First, the annealing temperature used by SF (450 and 480 °C during sulfurization) were lower than that used in this work, and a longer sulfurization time was also applied with Ar gas. In addition, the SF used a high H₂S gas concentrations of 10, 15, and 20% under continuous selenization [7]. Therefore, it is critical to optimize the sulfurization process to further increase the efficiency of these films. In this study, the sulfur concentration was controlled by changing the ratio of the H₂S and N₂ gases, as shown in Figures 1(b) and 1(c). These two-step process variations can be used to gain an optimal double-graded bandgap in the CIGSSe absorber layer, and the details of the bandgap depth profiles are shown in Supplementary Figure S1. The results indicate that we can achieve the highest efficiency of 15.85% with a solar cell aperture area of 878.6 cm². Table I indicates the device characteristics for the two-step-sulfurized CIGSSe solar cells when cell parameters were obtained using a 300 × 300-mm² monolithic module.

3.2. Characterization of phases in CIGSSe

Figure 2 displays the phase distribution depth profile obtained with the micro Raman scattering spectra of the two-step-sulfurized films with a low S concentration [Figures 2(a) and 2(c)] and a high S concentration [Figures 2(b) and 2(d)] in the first sulfurization step. We selected 12 locations from the surface to near the back contact layer, including the S-rich and Se-rich spots. The surface sulfurization process was applied to these CIGSSe films, so the ratio of S/(S+Se) at the surface of the absorber layer is higher than that in the middle. In addition, the intensity of the A₁ mode near the 292-cm⁻¹ peak is associated with anion (S or Se) vibration and hence related to the S concentration [16–19], so we can expect a higher intensity of the CuInS₂ (CIS) peak at 292 cm⁻¹ as the S concentration increases in the CIGSSe absorber layer. CIGSSe films with high [Figure 2(d)] S concentrations exhibit a main CIGSSe peak that appears at spots 1 to 12. The CIS A₁ mode is strongly influenced by the

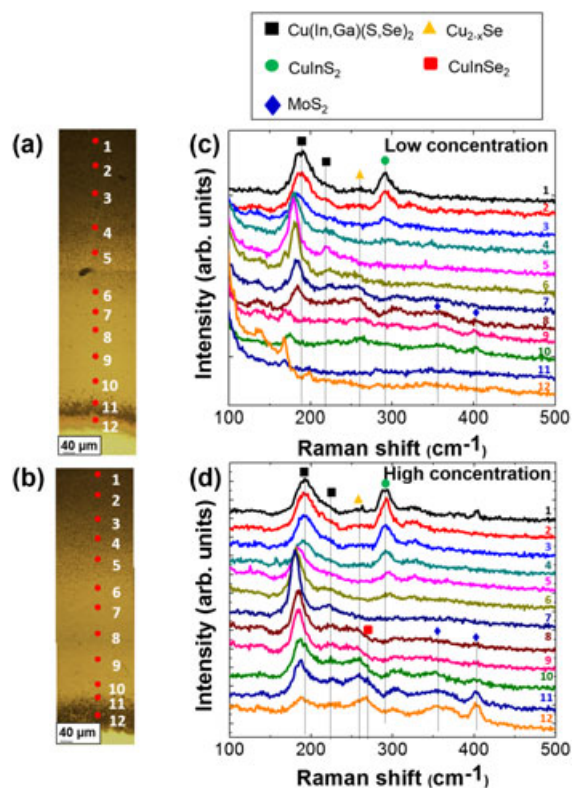


Figure 2. Optical images and Raman spectra of the two-step-sulfurized CIGSSe thin films. The locations from where Raman measurements were obtained are marked for the samples with (a) low and (b) high concentrations of sulfur. Depth profile Raman spectra of the films with a (c) low and (d) high S concentration. It can be seen in (c) that the main CIGSSe peak (black square) disappears as the depth progresses from spot 1 to 8, while in (d) the main CIGSSe peak remains throughout the depth from spots 1 to 12, indicating that the CIGSSe phase exists in the entire absorber layer region. The A₁ mode CIS peak (green circle) can also be seen in more sampling spots in (d) than in (c).

composition of the chalcopyrite compound. The vibrational motion of S and Se atoms (VI) directly affects the CIS A₁-mode frequency, and that of Ga and In (III) is associated with the CIGSSe A₁-mode frequency near 190 cm⁻¹ [17–19]. Furthermore, the frequency of the A₁ mode can be calculated from the weight ratio of I, II, and VI group elements of CIGSSe. The A₁ mode CIS peak appears at spots 1 to 6 in the high S concentration CIGSSe film [Figure 2(d)]. The CIS peak shifts linearly from 294 to

Table I. Module (30 × 30 cm²) parameters for the CIGSSe thin film solar cells.

Sulfurization process	Sulfur concentration		Efficiency (%)	V _{OC} (V)	J _{SC} (mA/cm ²)	Fill Factor (%)	R _{series} (Ω/cm ²)	R _{shunt} (Ω/cm ²)	A
	1	2							
two-step	0.05:10	1:10	14.68	0.626	33.62	69.71	1.25	644	1.60
	0.2:10	1:10	15.85	0.683	31.86	72.82	1.19	1473	1.47

Parameters include efficiency, open-circuit voltage (V_{OC}), short circuit current (J_{SC}), fill factor, series resistance (R_{series}), shunt resistance (R_{shunt}) and diode ideality factor (A). The best device exhibits a conversion efficiency of 15.85% from a two-step sulfurized CIGSSe thin film.

290 cm⁻¹ with changing S/(S+Se) concentration, as indicated in Table II [20–29]. Table II also shows that the CIGSSe A₁-mode peak exhibited a linear frequency shift that reflects the change in Ga/(Ga+In) ratio. The film with low S concentration [Figure 2(c)] only exhibited the CIS peak in the spectra measured at spots 1 to 4 because of the insufficient S incorporation. These results indicate that the process using a high S concentration provides sufficient S incorporation and forms a high-quality CIGSSe absorber layer. The CIS A₁ mode is influenced by the S/(S+Se) ratio because of the vibration of the anion sublattice [18,20]. The A₁-mode frequency is inversely proportional to anion atomic weight [17,19]. Thus, the MoS₂ peak is broader for the CIGSSe film with a high S concentration than that of the film with a low S concentration.

Figure 3 exhibits transmission electron microscopy cross-section images [Figures 3(a) and 3(d)] and the corresponding EDS maps for sulfur [Figures 3(b) and 3(e)] and selenium [Figures 3(c) and 3(f)] in the two-step-sulfurized CIGSSe thin films. The high intensity of the S EDS map can be seen at the surface of the high S concentration CIGSSe thin film. The Se is uniformly distributed in the CIGSSe thin film with a low S concentration, while the high S concentration film exhibits a Se intensity that is lower at the surface of film. EDS results

revealed that S diffuses into the deeper layers of the CIGSSe with a high S concentration and accumulates at the surface of the CIGSSe layer with high S concentration, while Se is distributed uniformly in the CIGSSe layers for both the high and low S concentration films.

Figure 4 plots the depth profile of the peak position of the work function distribution of the two-step-sulfurized CIGSSe thin films with different S concentrations at different spots (1 to 8) from the CIGSSe surface to the Mo layer. At spot “1” at the surface of the CIGSSe absorber layer, the high S concentration film exhibits a higher work function value than the low S concentration film, while the work function value of the CIGSSe film increases near the back contact. The work functions of the two-step-sulfurized CIGSSe thin films with different sulfur concentrations were calculated by comparing the work functions of the tip and the sample. The work function of the sample (ϕ_{sample}) was obtained by subtracting the tip work function (ϕ_{tip}) and by using highly-oriented pyrolytic graphite [14,15], though its value is affected by the doping and carrier concentration [30–35]. V_{CPD} is the contact potential difference of the tip and the sample, and e is the elementary charge. Specifically, the work function changes when the Fermi level changes with lower doping concentrations, so a higher S concentration induces an increase in the work function. The scan size

Table II. Depth-dependent Raman scattering spectra peak locations of different phases in the CIGSSe thin films [21–29].

Spot	two-step: low concentration (cm ⁻¹)				two-step: high concentration (cm ⁻¹)				
	CIGSSe	Cu _{2-x} Se	CuInS(Se) ₂	MoS ₂	CIGSe	Cu _{2-x} Se	CuInS(Se) ₂	MoS ₂	
1	191.28	259.99	291.49		192.91	262.34	291.49		
	211.02				214.23				
2	188.94	260.74	292.35		191.30		293.09		
	218.94				215.84				
3	182.62		290.74		192.16		290.74		
	214.23				216.59				
4	179.48		294.71		189.80		291.49		
	218.20				215.84				
5	179.51				184.98		294.71		
	217.34				213.37				
6	180.26	256.77			182.62		295.46		
	222.05				216.59				
7	182.62	257.62	308.10	361.79	181.12				
	224.52				220.55				
8	183.48	257.63	306.49	362.54	184.23	256.77			
	223.66				223.66				
9		264.70	270.27	364.14	184.23		256.02		
			305.74						
			170.08						401.97
			223.66						
10		263.09	173.94	303.52	185.83		270.27		
			363.29						224.52
			401.97						259.99
11			169.22	302.53	186.58		271.02	363.28	
			227.63						302.53
12			166.87	303.39	187.33		271.15	364.89	
			220.55						404.33

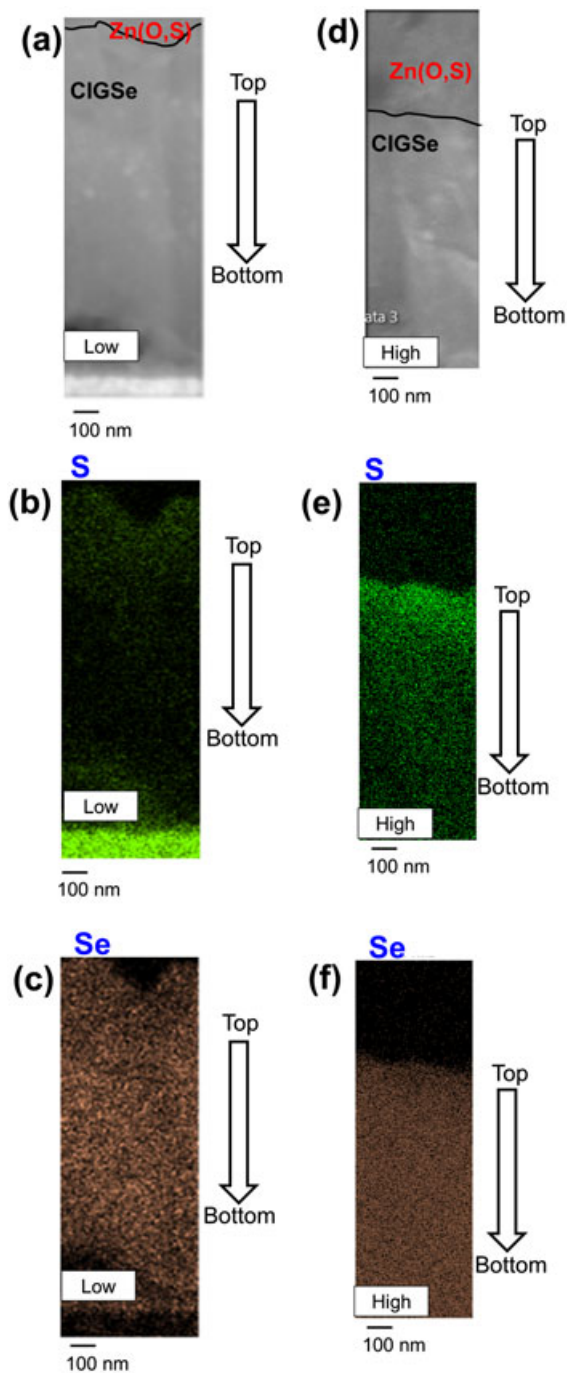


Figure 3. Transmission electron microscope cross-section images of two-step-sulfurized CIGSSe thin films with (a) low and (d) high S concentration. Energy-dispersive X-ray spectra elemental maps showing the distribution of (b,e) S and (c,f) Se in the CIGSSe absorber layer. (e) The high intensity of S is apparent near the surface of the sample with high S concentration.

of the KPFM images is of $3 \times 3 \mu\text{m}^2$, and the grain size for CIGSSe is about 100–200 nm, as indicated in Supplemental Figures S2 and S3. Dimpled samples were prepared

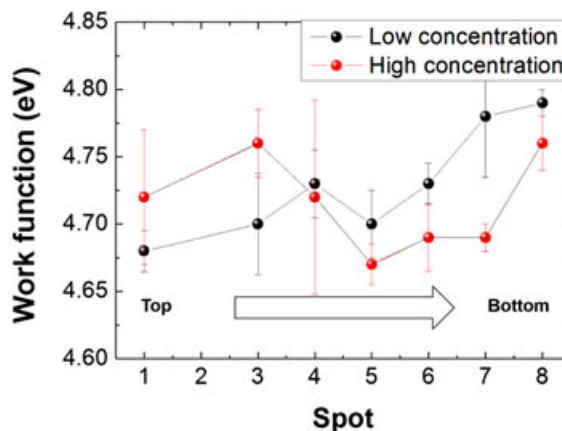


Figure 4. The depth profile work function distribution of the two-step-sulfurized CIGSSe thin films processed with low and high S concentrations, showing the peak position of the work function from different depth locations (spot) from the CIGSSe surface to the Mo layer. At the surface of the CIGSSe absorber layer (spot “1”), the film with a high S concentration exhibits a higher work function value than the low S concentration film. The work function values increase near the back contact (spot “8”).

with alumina nanoparticles and were subsequently etched with deionized water for 10 min to remove the oxidation layer. Baier *et al.* reported that the work function of an as-grown (1 h exposed to air) CIGS sample was ~ 4.4 eV, and that of a chemically etched CIGS sample was ~ 4.8 eV [15]. Our work function value for the CIGSSe samples averaged ~ 4.72 eV with deionized water etching, and this corresponds to the values presented by the other groups. When the sample was sulfurized in non-optimal sulfurization concentrations, the sulfur could not react well with the CIGSSe film. As a result, a secondary phase formed in the CIGSSe absorber layer that possessed a non-uniform composition [31,32]. In the surface of the absorber layer, the low S concentration CIGSSe film exhibits work function values that are lower than the high S concentration film at spots “1” and “2.” However, at spot “4,” the work function value for the low S concentration film is higher than that of the high S concentration film. In the middle of the absorber layer, the work function value is similar for both of the CIGSSe films. We should mention that Ga and S influenced the work function of the CIGSSe thin films. In a previous study, the work function of GBs in CIGSe absorber layer did not depend on Ga content [15]. However, a correlation between the work function and S/(S+Se) composition ratio of $\text{Cu}_2\text{ZnSn}(\text{S,Se})_4$ (CZTSSe) was observed in KPFM measurements [33]. An increase in the S/(S+Se) ratio raised the local work function, consistent with the presence of S-rich regions in CZTSSe. Based on these previous studies, we expect that the S/(S+Se) ratio plays a larger role than the Ga/(Ga+In) ratio in determining the work function of the CIGSSe films. The details of the work function values are given in Supplemental Figure S4.

4. DISCUSSION

4.1. Phase distribution of CIGSSe as a function of S concentration

Figure 5 schematically displays the S grading and the phase distribution of the two-step-sulfurized CIGSSe thin films with a low S concentration [Figure 5(a)] and a high S concentration [Figure 5(b)]. The dark grey gradation region marked in the high S concentration CIGSSe thin film indicates that deeper sulfur diffusion exists in this film than what exists in the low S concentration thin film. The Se is uniformly distributed in the CIGSSe layer, and S is accumulated near the surface of the CIGSSe absorber layer. In particular, higher amounts of sulfur are contained near the surface of the two-step-sulfurized CIGSSe layer with a high S concentration, as indicated in Figure 5(b). Based on the Raman scattering spectra, we can expect that thicker Cu_{2-x}Se phase exist in the CIGSSe layer with a low S concentration than that with a high S concentration.

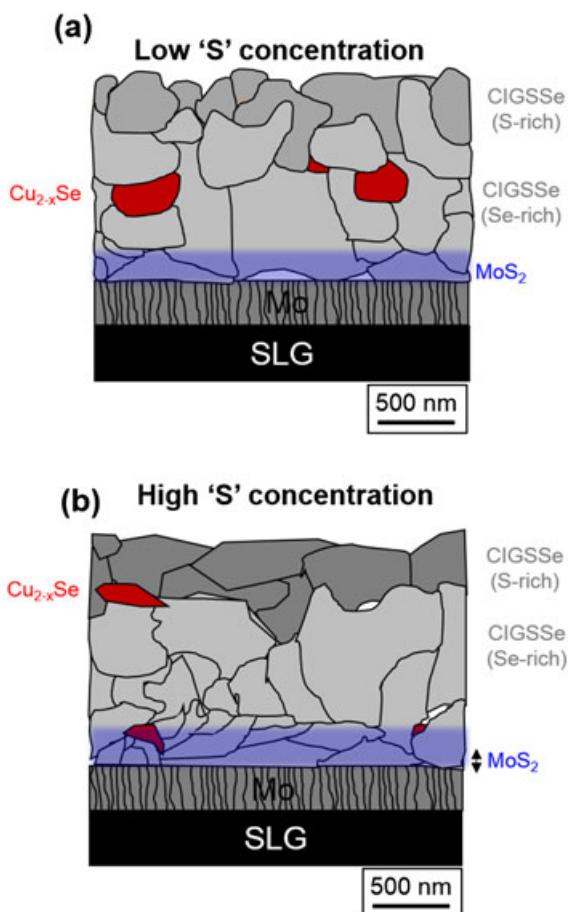


Figure 5. Schematic of the S grading and phase distribution of the two-step sulfurized CIGSSe thin film with (a) low and (b) high S concentrations. The schematic (b) demonstrates deeper sulfur diffusion (dark grey area) in the film with a high S concentration than that with a (a) low S concentration.

4.2. Device characteristics

Figure 6(a) indicates the current versus voltage curves of the CIGSSe thin film solar cells with the different two-step sulfurization processes with two different S concentrations. The CIGSSe film with high S concentration prepared by two-step sulfurization exhibits a better V_{OC} than that of the film with low S concentration. The work function distributions of the surface of the CIGSSe thin films with different S concentrations measured by KPFM are shown in Supplemental Figure S5. A high S concentration gave a more uniform work function distribution than a low S concentration. We previously reported a similar result that uniform surface phase distributions, indicated by a sharp work function distribution, correspond with uniform phase formation and better crystallinity of CIGSSe [12]. Based on

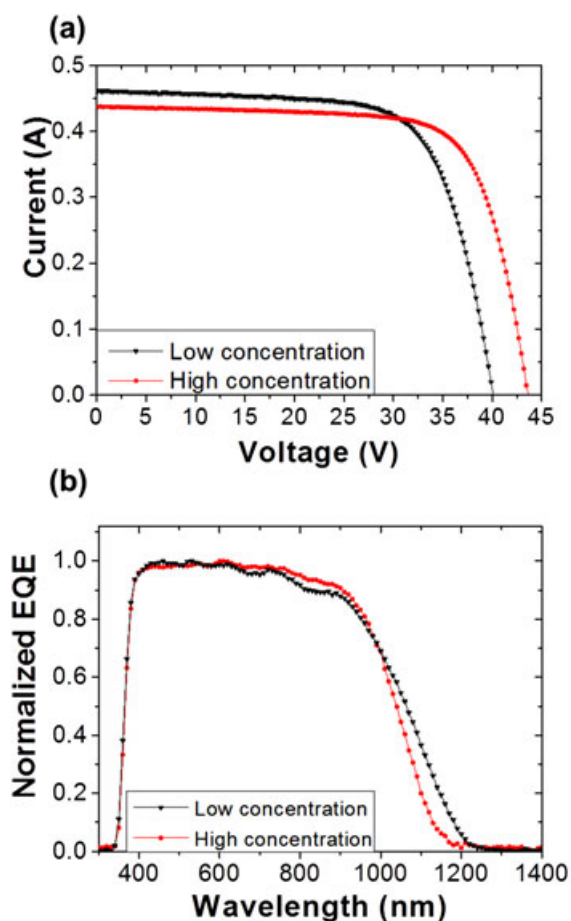


Figure 6. (a) Current–voltage curves of double-graded CIGSSe thin film solar cells with different S concentrations. The highest conversion efficiency is found for the cell containing a thin film with high S concentration prepared by two-step sulfurization. (b) External quantum efficiency (EQE) measurements of CIGSSe thin films with different S concentrations prepared by two-step sulfurization. The cell with a CIGSSe film with high S concentration exhibits the highest quantum efficiency of those investigated.

this, the CIGS_{Se} surface with uniform phase distribution should form a better contact with the buffer layer than the one with non-uniform phase distribution. Figure 6(b) plots the external quantum efficiency of the CIGS_{Se} thin film solar cells sulfurized with a two-step process for two different S concentrations. In this plot, the high S concentration of the CIGS_{Se} thin film solar cell exhibits better quantum efficiency than that of the low S concentration solar cell. The calculated J_{SC} for the cells containing films with low and high sulfur concentration are 38.40 and 38.02 mA/cm², respectively. These results correspond with the I-V data (J_{SC} of the devices containing films with low and high sulfur concentration were 33.62 and 31.86 mA/cm², respectively). The calculated bandgaps of the films with low and high sulfur concentrations are 1.17 and 1.21 eV, respectively. The bandgap difference affects J_{SC} , and thus the device containing a film with high sulfur concentration shows a lower J_{SC} than that of the device with a film with low sulfur concentration. The device containing a CIGS_{Se} film with high sulfur concentration shows higher external quantum efficiency than that of the device with a film with low sulfur concentration because of the better bulk quality of the CIGS_{Se} film with high sulfur concentration. Moreover, scanning emission microscopy images of the cross-section for both of these thin films shows that the high S concentration film possesses dense grains near the back contact region, while the low S concentration film possesses porous grains near the Mo layer (Supplemental Figure S6). The uniform grain growth influences to the better contact under high S concentration. It could improve the fill factor of the optimized two-step CIGS_{Se} device. Moreover, the optimized two-step sulfurization process obtained uniform phase distribution of CIGS_{Se} layer and double graded bandgap profile within CIGS_{Se} absorber layer. It results in better quantum efficiency of absorber layer and interface quality. Therefore, the double-graded bandgap improves the V_{OC} , fill factor, and absorption of the CIGS_{Se} thin film solar cell.

5. CONCLUSIONS

We obtained a double-graded bandgap CIGS_{Se} module by sputtering and annealing in the presence of S and Se-containing gases. The highest conversion efficiency was of 15.85% with an aperture area of 878.6 cm². Micro-Raman spectroscopy and Kelvin probe force microscopy were used to investigate the optical and electrical properties of the phase distribution and phase formation as a function of the depth for the absorber layer that was prepared with different sulfur concentrations. A two-step-sulfurized CIGS_{Se} thin film possessing a relatively high sulfur concentration exhibits a deeper sulfur diffusion and thinner Cu_{2-x}Se phase than that with a lower S concentration. The depth profile of the Raman spectra, the main CIGS_{Se} peaks, and the CIS peaks of the two-step-sulfurized CIGS_{Se} thin film that possesses a higher

sulfur concentration evidenced the existence of larger phase areas and better crystallinity. The CIGS_{Se} surface with uniform phase distribution should form a better contact with the buffer layer than the one with non-uniform phase distribution. The bandgap difference affects J_{SC} , and thus the device containing a film with high sulfur concentration shows a lower J_{SC} than that of the device with a film with low sulfur concentration. The device containing a CIGS_{Se} film with high sulfur concentration shows higher external quantum efficiency than that of the device with a film with low sulfur concentration because of the better bulk quality of the CIGS_{Se} film with high sulfur concentration. Therefore, we can expect this more uniform surface phase improves the interface state between CIGS_{Se} and Zn (O,S) in terms of the V_{OC} .

ACKNOWLEDGEMENTS

This work was supported by the New and Renewable Energy of the Korea Institute of Energy Technology Evaluation and Planning (KETEP), with a grant funded by the Korea government, Ministry of Trade, Industry and Energy (No. 20123010010130).

REFERENCES

1. "Solar frontier achieves world record thin-film solar cell efficiency: 22.3%" [Online]. Available: <http://www.solar-frontier.com/eng/new/2015/C051171.html>. Accessed: January 15, 2016.
2. Green MA, Emery K, Hishikawa Y, Warta W, Dunlop ED. Solar cell efficiency tables (version 45). *Progress in Photovoltaics: Research and Applications* 2015; **23**: 1–9.
3. Dullweber T, Hanna G, Rau U, Shock HW. A new approach to high-efficiency solar cells by band gap grading Cu(In,Ga)Se₂ chalcopyrite semiconductors. *Solar Energy Materials and Solar Cells* 2001; **67**: 145–150.
4. Gloeckler M, Sites JR. Band-gap grading in Cu(In,Ga)Se₂ solar cells. *Journal of Physics and Chemistry of Solids* 2005; **66**: 1891–1894.
5. Gloeckler M, Sites JR. Efficiency limitations for wide-bandgap chalcopyrite solar cells. *Thin Solid Films* 2005; **480-481**: 241–245.
6. Huang CH. Effects of Ga content on Cu(In,Ga)Se₂ solar cells studied by numerical modeling. *Journal of Physics and Chemistry of Solids* 2008; **69**: 330–334.
7. Nagoya Y, Kushiya K, Tachiyuki M, Yamase O. Role of incorporated sulfur into the surface of Cu(In,Ga)Se₂ thin-film absorber. *Solar Energy Materials and Solar Cells* 2001; **67**: 247–253.

8. Goushi Y, Hakuma H, Tabuchi K, Kijima S, Kushiya K. Fabrication of pentanary Cu(InGa)(SeS)₂ absorbers by selenization and sulfurization. *Solar Energy Materials and Solar Cells* 2009; **93**: 1318–1320.
9. Nam J, Kang Y, Lee D, Yang JY, Kim YS, Mo CB, Park S, Kim D. Achievement of 17.9% efficiency in 30x30 cm² Cu(In,Ga)Se₂ solar cell sub-module by sulfurization after selenization with Cd-free buffer. *Progress in Photovoltaics: Research and Applications* 2015. DOI:10.1002/pp.2653.
10. Fontané X, Izquierdo-Roca V, Calvo-Barrio L, Pérez-Rodríguez A, Morante JR, Guettler D, Eicke A, Tiwari AN. Investigation of compositional inhomogeneities in complex polycrystalline Cu(In,Ga)Se₂ layers for solar cells. *Applied Physics Letters* 2009; **95**: 261912.
11. Fontané X, Izquierdo-Roca V, Calvo-Barrio L, Álvarez-García J, Pérez-Rodríguez A, Morante JR, Witte W. In-depth resolved Raman scattering analysis of secondary phases in Cu-poor CuInSe₂ based thin films. *Applied Physics Letters* 2009; **95**: 121907.
12. Yang JY, Lee D, Huh KS, Jung SJ, Lee JW, Lee HC, Baek DH, Kim BJ, Kim D, Nam J, Kim GY, Jo W. Influence of surface properties on the performance of Cu(In,Ga)(Se,S)₂ thin film solar cells using Kelvin probe force microscopy. *RSC Advances* 2015; **5**: 40719.
13. Yang JY, Nam J, Kim D, Kim GY, Jo W, Kang Y, Lee D. Enhancement of the photo conversion efficiencies in Cu(In,Ga)(Se,S)₂ solar cells fabricated by two-step sulfurization process. *Applied Physics Letters* 2015; **107**: 193901.
14. Melitz W, Shen J, Kummel AC, Lee S. Kelvin probe force microscopy and its application. *Surface Science Reports* 2011; **66**: 1–27.
15. Baier R, Lehmann J, Lehmann S, Rissom T, Kaufmann CA, Schwarzmann A, Rosenwaks Y, Lux-Steiner MC, Sadewasser S. Electronic properties of grain boundaries in Cu(In,Ga)Se₂ thin films with various Ga-contents. *Solar Energy Materials and Solar Cells* 2012; **103**: 86–92.
16. Witte W, Kniese R, Powalla M. Raman investigations of Cu(In,Ga)Se₂ thin films with various copper contents. *Thin Solid Films* 2008; **517**: 867–869.
17. Roy S, Guha P, Kundu SN, Hanzawa H, Chaudhuri S, Pal AK. Characterization of Cu(In,Ga)Se₂ films by Raman scattering. *Materials Chemistry and Physics* 2002; **73**: 24–30.
18. Kodigala S. Cu(In_{1-x}Ga_x)Se₂ based thin film solar cells. *Thin Films and Nanostructures* 2010; **35**: 276–306.
19. Jeong AR, Jo W, Song M, Yoon S. Crystalline ordered states of CuIn_{1-x}Ga_xSe₂ (x = 0, 0.3, and 1.0) thin-films on different substrates investigated by Raman scattering spectroscopy. *Materials Chemistry and Physics* 2012; **134**: 1030–1035.
20. Oh Y, Yang W, Kim J, Woo K, Moon J. Aqueous solution-phase selenized CuIn(S,Se)₂ thin film solar cells annealed under inert atmosphere. *Applied materials and interfaces* 2015; **7**: 22570–22577.
21. Han J, Ouyang L, Zhuang D, Liao C, Liu J, Zhao M, Cha L, Besland MP. Raman and XPS studies of CIGS/Mo interfaces under various annealing temperatures. *Materials Letters* 2014; **136**: 278–281.
22. Park SU, Sharma R, Sim JK, Baek BJ, Ahn HK, Kim JS, Lee CR. Development of gold induced surface plasmon enhanced CIGS absorption layer on polyimide substrate. *Applied Surface Science* 2013; **280**: 757–763.
23. Cho A, Ahn SJ, Yun JH, Gwak J, Ahn SK, Shin K, Yoo J, Song HJ, Yoon KH. The growth of Cu_{2-x}Se thin films using nanoparticles. *Thin Solid Films* 2013; **546**: 299–307.
24. Bourlier Y, Robbe OC, Lethien C, Roussel P, Pastre A, Zegaoui M, Rolland N, Bouzaoui M, Rémy Bernard R. Control of gallium incorporation in sol-gel derived CuIn_{1-x}Ga_xS₂ thin films for photovoltaic applications. *Materials Research Bulletin* 2015; **70**: 137–144.
25. Yakushev MV, Mudryi AV, Victorov IV, Krustok J, Mellikov E. Energy of excitons in CuInS₂ single crystals. *Applied Physics Letters* 2006; **88**: 011922.
26. Lee DY, Kim JH. Characterization of sprayed CuInS₂ films by XRD and Raman spectroscopy measurements. *Thin Solid Films* 2010; **518**: 6537–6541.
27. Rincon C, Ramirez FJ. Lattice vibrations of CuInSe₂ and CuGaSe₂ by Raman microspectrometry. *Journal of Applied Physics* 1992; **72**: 4321.
28. Gofasa K, Grzeszczyk M, Bozek R, Leszczyński P, Wyszomolek A, Potemski M, Babiński A. Resonant Raman scattering in MoS₂—from bulk to monolayer. *Solid State Communications* 2014; **197**: 53–56.
29. Fernandes PA, Salomé PMP, da Cunha AF. Study of polycrystalline Cu₂ZnSnS₄ films by Raman scattering. *Journal of Alloys and Compounds* 2011; **509**: 7600–7606.
30. Kim GY, Jo W, Lee KD, Choi HS, Kim JY, Shin HY, Nguyen TTT, Yoon S, Joo BS, Gu M, Han M. Optical and surface probe investigation of secondary phases in Cu₂ZnSnS₄ films grown by electrochemical deposition. *Solar Energy Materials and Solar Cells* 2015; **139**: 10–18.
31. Glatzel T, Marrón DF, Schedel-Niedrig T, Sadewasser S, Lux-Steiner MC. CuGaSe₂ solar cell cross section studied by Kelvin probe force microscopy in ultrahigh vacuum. *Applied Physics Letters* 2002; **81**: 2017.

32. Glatzel T, Steigert H, Sadewasser S, Klenk R, Lux-Steiner MC. Potential distribution of Cu(In,Ga)(S,Se)₂-solar cell cross-sections measured by Kelvin probe force microscopy. *Thin Solid Films* 2015; **480**: 177–182.
33. Salvador M, Vorpahl SM, Xin H, Williamson W, Shao G, Karatay DU, Hillhous HW, Ginger DS. Nanoscale surface potential variation correlates with local S/Se ratio in solution-processed CZTSSe solar cells. *Nano Letters* 2014; **14**: 6926–6930.
34. Lifshitz N. Dependence of the work-function difference between the polysilicon gate and silicon substrate on the doping level in polysilicon. *IEEE Transactions on Electron Devices* 1985; **32**: 617–621.
35. Kim GY, Son DH, Nguyen TTT, Yoon S, Kwon M, Jeon CW, Kim DW, Kang JK, Jo W. Enhancement of photo-conversion efficiency in Cu₂ZnSn(S,Se)₄ thin-film solar cells by control of ZnS precursor-layer thickness. *Progress in Photovoltaics: Research and Applications* 2016; **24**: 292–306.

SUPPORTING INFORMATION

Supporting information may be found in the online version of this article.